The Cryosphere Discuss., 9, 4661–4699, 2015
www.the-cryosphere-discuss.net/9/4661/2015/
doi:10.5194/tcd-9-4661-2015

The Cryosphere Discussions
Open Access

Improved GRACE regional mass balance estimates of the Greenland Ice Sheet cross-validated with the input-output method

Z. Xu[1], E. Schrama[1], W. van der Wal[1], M. van den Broeke[2], and E. M. Enderlin[3]

[1]Faculty of Aerospace Engineering, Delft University of Technology, the Netherlands
[2]Institute for Marine and Atmospheric Research, Utrecht University (UU/IMAU), the Netherlands
[3]Climate Change Institute & School of Earth and Climate Science, University of Maine, Orono, ME 04469, USA

Received: 1 August 2015 – Accepted: 14 August 2015 – Published: 4 September 2015

Correspondence to: Z.Xu (Z.Xu-1@tudelft.nl)

Published by Copernicus Publications on behalf of the European Geosciences Union.

Abstract

In this study, we use satellite gravimetry data from the Gravity Recovery and Climate Experiment (GRACE) to estimate regional mass changes of the Greenland ice sheet (GrIS) and neighbouring glaciated regions using a least-squares inversion approach. We also consider results from the input-output method (IOM) that quantifies the difference between mass input and output of the surface mass balance (SMB) components from the Regional Atmospheric Climate Model version 2 (RACMO2) and ice discharge (D) from 12 years of high-precision ice velocity and thickness surveys.

We use a simulation model to quantify and correct for GRACE approximation errors in mass changes between different sub-regions of GrIS and investigate the reliability of pre-1990s ice discharge estimates based on modelled runoff. We find that the difference between IOM and our improved GRACE mass change estimates is reduced in terms of the long-term mass changes when using runoff-based discharge estimates in several sub-areas. In most regions our GRACE and IOM solutions are consistent with other studies, but differences remain in the northwestern GrIS. We verify the GRACE mass balance in that region by considering several different GIA models and mass change estimates derived from the Ice, Cloud and land Elevation satellite (ICEsat). We conclude that the remaining differences between GRACE and IOM are likely due to underestimated uncertainties in the IOM solutions.

1 Introduction

During the last decade, the ice mass loss from the Greenland ice sheet (GrIS) became one of the most significant mass changing events on Earth. Because of its ongoing and potentially large future contribution to sea level rise, it is critical to understand the mass balance of the GrIS in detail. As the result of increasing run-off and solid ice discharge, the GrIS has been experiencing a considerable and increasing mass loss since the mid-1990s (Hanna et al., 2005; Rignot and Kanagaratnam, 2006; van den

TCD
9, 4661–4699, 2015

Broeke et al., 2009). The changes in mass loss rates are due to different processes, e.g. in the northwestern GrIS the mass loss acceleration is linked to the rapidly increasing discharge in this region (Andersen et al., 2014; Enderlin et al., 2014), while in the southeast the increase in mass loss rate after 2003 is mainly due to enhanced melting and less snowfall (Noël et al., 2015).

To quantify recent changes in GrIS mass balance, three methods are used: satellite altimetry, satellite gravimetry and the input-output method (Andersen et al., 2015; Colgan et al., 2014; Sasgen et al., 2012; Shepherd et al., 2012; Velicogna et al., 2014; Wouters et al., 2013). The latter two methods are briefly discussed in the following.

The input/output method (IOM) evaluates the difference between mass input and output for a certain region. For the GrIS, precipitation (P) in the form of snowfall is the main contribution to the mass input, while mass loss is a combination of sublimation (S), melt water runoff (R), and solid ice discharge (D). Surface mass balance (SMB) equals to P-S-R, and subtracting D from SMB yields the total mass balance (TMB). SMB is commonly estimated using climate models with high resolution in the spatial ($\sim 0.05^{\circ} \sim 0.25^{\circ}$) and time domains (hourly to daily), (Ettema et al., 2009; Fettweis, 2007; Tedesco et al., 2013; Van Angelen et al., 2012). Ice discharge can be estimated with combined measurements of ice velocity and the ice thickness, e.g. Rignot and Kanagaratnam (2006), Enderlin et al. (2014) and Andersen et al. (2015). In the IOM, sometimes the 1961 to 1990 reference SMB is used to estimate missing D estimations in some regions (Sasgen et al., 2012) assuming that mass gain from surface mass balance during that period is compensated by ice discharge (i.e., no mass change). One can also obtain TMB from SMB and D without using a reference period, e.g. Andersen et al. (2015), but this method may also indicate in unrealistic mass gains or losses if we accumulate the TMB over a long time period (van den Broeke et al., 2009). By removing the reference the influence of the large uncertainties and inter-annual variability in SMB and D can be reduced (van den Broeke et al., 2009). We will discuss the details of both IOM versions in Sect. 2.

TCD
9, 4661–4699, 2015

The satellite gravity observations from GRACE (Gravity Recovery and Climate Experiment), provide spherical harmonic coefficients of the global gravity field for each month since the end of 2002. By converting the spherical harmonic coefficients of the GRACE monthly gravity field to changes in mass at a layer on the Earth's surface, one can obtain the 2-D monthly mass changes. GRACE observations are, however, influenced by measurement noise and leakage of signals caused by mass changes in neighbouring areas. Finally, the GRACE data contain north-south directed stripes due to measurement noise and mis-modeled high-frequency signal aliasing in the monthly gravity fields.

By employing the inversion approach, one can estimate the mass balance for GrIS sub-regions from GRACE data. Comparing the GRACE solution with the IOM shows that differences exist for some regions in the southeast or in the northwest (see Fig. A1 in the Appendix) while on larger scales, e.g. the entire GrIS, estimates usually agree well (Sasgen et al., 2012; Shepherd et al., 2012). Part of the regional differences arises from the inversion approach that is applied to the GRACE data. Bonin and Chambers (2013) found that applying the Least Squares inversion method (Schrama and Wouters, 2011) to a simulation of the GrIS mass change produced mass balance estimates that differed from the simulated mass change. Another part of the regional differences is assumed to be related with the uncertainty in discharge estimates (Sasgen et al., 2012).

In this study, we aim to tackle both sources of uncertainty. (i) We present a way to reduce the error from the inversion approach and (ii) we investigate different discharge estimates. We then evaluate our results by comparing GRACE and IOM estimates with each other and with published estimates from satellite altimetry. Previous studies have compared regional GrIS mass changes from different independent methods. In Sasgen et al. (2012), the mass balance in 7 major GrIS basins was derived from the IOM and GRACE data using a forward modelling approach (Sasgen et al., 2010). When separating out the IOM components and comparing with the seasonal variability in the derived GRACE solution, the importance of each IOM component to annual total

TCD
9, 4661–4699, 2015

mass changes was revealed. In the northwestern GrIS important differences between IOM and GRACE were noted, which were ascribed to the uncertainty in the regional discharge component in this area where detailed surveys of ice thickness are lacking. The comparison between two approaches shows $24 \pm 13\,\mathrm{Gt\,yr^{-1}}$ mass loss difference in this region, and as a result the uncertainty in the regional mass balance estimate is estimated at ∼ 46 %. However, using new discharge estimates and the corresponding IOM regional mass changes in the northwestern GrIS, Andersen et al. (2015) found that the difference between GRACE and IOM mass loss estimates fell within the combined uncertainty range. Using the Least Squares based inversion approach of Schrama and Wouters (2011), we find that the mass change differences between GRACE and IOM in the southern GrIS increase and cannot be explained by the assumed uncertainties. An example of the regional difference between the GRACE data and the IOM solution can be seen in Fig. A1 in the Appendix. The details of this difference will be discussed in Sect. 4.

In order to find regional mass balance on 8 major GrIS drainage systems (DS) according to the definition of Zwally (2012) with each DS further separated into a coastal region and an interior region divided by the 2000 m elevation contour line. This GrIS DS definition is employed by several other studies, (Andersen et al., 2015; Barletta et al., 2013; Colgan et al., 2014; Luthcke et al., 2013; Sasgen et al., 2012). Also, Wouters et al. (2008) found that in GRACE data, the regional mass changes on GrIS are also influenced by the mass changes in areas outside Greenland, i.e. Ellesmere Island, Baffin Island, Iceland and Svalbard (EBIS) (Wouters et al. 2008). Therefore, we include four additional DS to reduce the leakage from these regions; the overall mascon definition used in this study are shown in Fig. 1.

The main topic of this study is to provide improved GrIS regional mass balance estimates from GRACE and the IOM. We show that the improved GRACE solution brings down the regional differences between two mass changes estimates, mainly in the southeast GrIS region. Furthermore, we compare the GRACE solution with the IOM, which employs different reference discharge estimates, showing that the uncertainties

TCD
9, 4661–4699, 2015

in the reference discharge can result in underestimated mass loss rate in the IOM regional solution in particular in the northwest GrIS region.

In Sect. 2, we present SMB mass changes from a recently improved regional atmospheric climate model (RACMO2) (Noël et al., 2015) and discharge estimates of Enderlin et al. (2014), which are based on a near-complete survey of the ice thickness and velocity of Greenland marine-terminating glaciers. We investigate different methods to calculate mass changes in basins using the modelled SMB and D estimates. In section 3, we introduce the Least Squares inversion approach and identify the approximation errors in regional mass change estimates from GRACE data. In section 4, we compare mass change estimates from GRACE and IOM, and discuss remaining differences. Conclusions and recommendations are given in Sect. 5.

2 IOM method

2.1 SMB and D

In this study, we use the Regional Atmospheric Climate Model, version 3 (RACMO2.3) to model the SMB of the GrIS. RACMO2 (Ettema et al., 2009; Van Angelen et al., 2012; van den Broeke et al., 2009) is developed and maintained at the Royal Netherlands Meteorological Institute (KNMI) and has been adapted for the polar regions at the Institute for Marine and Atmospheric Research, Utrecht University (UU/IMAU). RACMO2 model output is currently available at $\sim 0.1^{\circ}$ spatial resolution for January 1958 to December 2014. The differences between a previous model version (RACMO2.1) and other SMB models are discussed by Vernon et al. (2013). In RACMO2 we assume 20 % uncertainties for the P and R components in each grid cell. Assuming both components to be independent, the uncertainty of the SMB is the quadratic sum of uncertainties of P and R. Note that the magnitude of S is small and its absolute uncertainty negligible compared to those in P and R.

TCD
9, 4661–4699, 2015

Ice discharge (D) estimates from Enderlin et al. (2014) (hereafter Enderlin-14, with the associated discharge estimates D-14) are used in this study. In Enderlin-14, the ice thickness of 178 glaciers is estimated as the difference in ice surface elevations from repeat digital elevation models and bed elevations from NASA's Operation IceBridge airborne ice-penetrating radar data while the ice surface velocity is obtained from tracking the movement of surface features visible in repeat Landsat 7 Enhanced Thematic Mapper Plus and the Advanced Spaceborne Thermal and Reflectance Radiometer (ASTER) images. For glaciers with thickness transects perpendicular to ice flow (i.e., flux gates), the ice flux is estimated by summing the product of the ice thickness and surface speed across the glacier width. Ice flux is estimated for glaciers with centreline or no thickness estimates using empirical scaling factors derived from the flux gate observations. Because the ice fluxes are calculated within 5 km of the estimated grounding line locations, no corrections are made to account for SMB gain/loss between the observations and the grounding lines and the ice discharge is estimated directly from the fluxes (Enderlin et al., 2014). The estimation of independent uncertainty of $1 \sim 5\,\%$ D for each glacier reduced the GrIS D uncertainty relative to previous studies, e.g. Rignot et al. (2008) (hereafter Rignot-08, and the associated estimates are denoted by D-08), which relied on interior ice thickness estimates that were assumed constant in time.

2.2 Cumulative TMB anomaly

For the whole GrIS or a complete basin from ice sheet maximum height to the coast, the total mass balance is:

$$\mathrm{TMB} = \mathrm{SMB} - \mathrm{D} \quad (1)$$

In this study, we further separate each GrIS basin in an upstream (up) and downstream (down) region relative to the 2000 m surface elevation contour line. For the sub-divided regions, Eq. (1) becomes:

$$\mathrm{TMB} = \mathrm{TMB}^{\mathrm{up}} + \mathrm{TMB}^{\mathrm{down}}. \quad (2)$$

TCD
9, 4661–4699, 2015

Where

$$\mathrm{TMB}^{\mathrm{up}} = \mathrm{SMB}^{\mathrm{up}} - F^{2000} \tag{3}$$

and

$$\mathrm{TMB}^{\mathrm{down}} = \mathrm{SMB}^{\mathrm{down}} + F^{2000} - F^{fg}. \tag{4}$$

F^{2000} refers to the ice flux across the 2000 m elevation contour, and F^{fg} refers to the ice flow across the flux gate. Note that F^{2000} is cancelled if the study area includes both the regions below and above the 2000 m contour, but the influence of this high elevation flux has to be considered when the interior region is studied separately. As described above, we assume that SMB changes downstream of the Enderlin-14 flux gates are negligible and that $F^{fg} = D$.

In order to fit the temporal resolution of the modeled SMB data, we interpolate the yearly D on a monthly basis. Significant seasonal variations in ice velocity have been observed along Greenland's marine-terminating outlet glaciers (Moon et al., 2014). However, since we focus mostly on long-term changes in mass in this study, monthly variations in D should have a negligible influence on our analysis and we assume that D is approximately constant throughout the year. The monthly GRACE data represent the gravity field of Earth at that particular month. By subtracting the gravity field from a reference period (e.g. the 2003–2014 average), the gravity variations with respect to this reference can be obtained. These can be converted to mass variations assuming that all mass variation takes place in a thin layer near to the Earth's surface. Contrary to the GRACE data, the SMB, D and TMB are estimates of rates of mass change (i.e., mass flux) in Gt/month or $\mathrm{Gt\,yr^{-1}}$. Hence in order to compare with GRACE, one has to integrate the SMB and D from a certain month (or year), which yields:

$$\delta\mathrm{TMB}_t = \int_{t_0}^{t} (\mathrm{SMB}_t - D_t)\mathrm{d}t, \tag{5}$$

TCD
9, 4661–4699, 2015

where $\delta \mathrm{TMB}_t$ is the cumulative mass change at month t in IOM (unit is Gt) and the integration time period is from the initial month t_0 to month t. $\delta \mathrm{TMB}_t$ also can be calculated with respect to a reference period during which D and SMB are equal or both known. Suppose during the reference period (1960–1990) the cumulative D and SMB are denoted by D_0 and SMB_0 then, Eq. (5) becomes:

$$\delta \mathrm{TMB}_t = (\mathrm{SMB}_0 - \mathrm{D}_0) + \int_{t_1}^{t_n} (\mathrm{SMB}_t - D_t)\mathrm{d}t \quad (6)$$

where $\mathrm{SMB}_t = \mathrm{SMB}_0 + \delta \mathrm{SMB}_t$ and $D_t = D_0 + \delta D_t$. Also note that the integration starts from the month t_1, which is January 1991 in this study. Compared to SMB_0, D_0 is more uncertain due to insufficient observations before 2000 (Rignot-08). One way to select the reference values is to assume that the GrIS was in balance during 1961 to 1990, so that during this period $\mathrm{SMB}_0 - D_0 = 0$ (e.g. van den Broeke et al., 2009; Sasgen et al., 2012).

As has been explained before, in order to investigate the regional mass balance for the regions below and above 2000 m, we substituting Eq. (3) and Eq. (4) into Eq. (6) separately, the ice flux across 2000 m contour has to be considered. Therefore we introduce two assumptions, i.e. (1) F^{2000} is constant over time, which means $F^{2000} = F_0^{2000}$ (F_0^{2000} is the F^{2000} during the reference period), so $\delta F^{2000} = 0$, and (2) the separate GrIS interior and coastal regions are all in balance during the 1961–1990 reference period, i.e. $\mathrm{SMB}_0^{\mathrm{up}} - \mathrm{D}_0^{\mathrm{up}} = 0$ and $\mathrm{SMB}_0^{\mathrm{down}} - \mathrm{D}_0^{\mathrm{down}} = 0$. Assumption (1) is necessary since there is a lack of yearly measurements of ice velocity across the 2000m contour. An estimate of decadal change by Howat et al. (2011) suggests it is reasonable to assume a constant F^{2000} for the entire GrIS, except for a few glaciers, such as the Jakobshavn glacier in basin 7 where the F^{2000} may be higher than F_0^{2000} after year 2000. In Andersen et al. (2015), the interior GrIS balance (in their study defined as the ice sheet above the 1700 m elevation contour) was 41 ± 61 Gt yr^{-1} during the 1960–1990 reference period and in Colgan et al. (2014) the interior flux was estimated as 54 ± 46 Gt yr^{-1} for the

TCD
9, 4661–4699, 2015

same time period, indicating the assumption of balance approximately holds within the uncertainties.

Based on these two assumptions, we apply Eq. (6) for the interior and coastal GrIS regions, yielding:

$$\delta \mathrm{TMB}_t^{\mathrm{up}} = \int_{t_1}^{t_n} (\mathrm{SMB}_t^{\mathrm{up}}) \mathrm{d}t \tag{7}$$

and

$$\delta \mathrm{TMB}_t^{\mathrm{down}} = \int_{t_1}^{t_n} (\mathrm{SMB}_t^{\mathrm{down}} - \mathrm{D}_t) \mathrm{d}t. \tag{8}$$

We quantify the combined uncertainties of assumption (1) and (2) by comparing the results from Eq. (8) to the mass balance using GRACE and ICEsat from Wouters and Schrama (2008) and Zwally et al. (2011), resulting in $\sim \pm 15\,\mathrm{Gt\,yr^{-1}}$ uncertainties. The regional uncertainties are summarized in Table A3 in the Appendix. Note that for each region, the same uncertainty is applied to both the interior and coastal areas. For the whole basin the uncertainties associated with assumption (1) and (2) will vanish, because these two assumptions are needed only when we separate the coastal and interior regions.

2.3 Reference SMB and D

In this study, the error in SMB_0, hereafter $\sigma\mathrm{SMB}_0$ involves the systematic error caused by the assumption of a reference period and the fact that averaging within the chosen reference period results in an error. Both parts will be explained hereafter.

The systematic error is the uncertainty in the SMB derived from model output and the averaging error is related to the variability of the reference SMB_0 during 1961–1990.

TCD
9, 4661–4699, 2015

To quantify the later, we apply a Monte-Carlo simulation to evaluate the standard deviations of the SMB_0 resulting from using different combinations of 20-year average of SMB. The sampled combinations are randomly chosen from the months between 1961 and 1990, following van den Broeke et al. (2009). For RACMO2, we find 20 Gt yr^{-1} averaging errors in σSMB_0. The SMB_0 from RACMO2 yields 403 Gt yr^{-1} hence the systematic error is approximately 73 Gt yr^{-1} (considering 18 % uncertainty in RACMO2). If we assume both errors are independent then $\sigma SMB_0 = 75$ Gt yr^{-1}.

We also investigate the uncertainties of the 1961–1990 reference discharge. In this study we employ D-14 as the D estimates in IOM. However D-14 time series starts from the year of 2000 when the GrIS already was significantly out of balance. In order to retrieve D_0 for D-14 ($D_0 - 14$), we employ the $D_0 = 413$ Gt yr^{-1} in 1996 from D-08 ($D_0 - 08$) for the entire GrIS, and assume that the regional D changes from 1990 to 2000 in D-08 should be proportion to the changes in D-14 in each region, i.e. D-14 and D-08 are linearly correlated. The details of the interpolation of regional D_0 are given in Appendix A1. Note that the averaging error in D_0 is minimized via an iteration process, the details can be found in Rignot et al. (2008). Due to the lack of ice thickness information before 2000, the reference D_0 in Rignot-08 has high uncertainty, especially in the northwest of the GrIS.

Another way to obtain historic discharge estimates is by using the presumed correlation between discharge and SMB or run-off (Rignot et al., 2008; Sasgen et al., 2012). The approach assumes that the anomaly of the discharge with respect to a reference SMB ($\delta D = SMB_0 - D$) is correlated with the anomaly of the 4-year averaging runoff with respect to a reference runoff ($\delta R = R - R_0$). In this study we choose to use the runoff output from the RACMO2 model. We consider three estimates of D, i.e. by Rignot-08, Enderlin-14 and Andersen et al. (2015), based on different measurements of the ice thickness and flux velocity changes, integration areas (areas between the flux gate and the grounding line), SMB and ice storage corrections and whether the peripheral areas are included or not. In this study we provide a runoff-based estimates for D_0 only those ice sheet basins where the correlation between δD and δR is strong (Fig. 2). For the

TCD
9, 4661–4699, 2015

entire GrIS, we obtain a high correlation ($R^2 = \sim 0.86$), similar to the correlation found by Rignot et al. (2008), but the regional correlations are lower and vary from 0.19 to 0.94. In DS 7 and DS 8, the discharge anomaly is obviously correlated with the runoff anomaly ($R^2 > 0.9$), while in other regions (i.e. in DS 2, DS 4, DS 5 and DS 6), the correlation is low ($R^2 < 0.5$). In DS 3a, when we consider only the D estimates from Enderlin-2014 and Andersen-2015, the correlation increases to $R^2 = 0.72$. Note that, the regions with high correlation are also those that have a large fraction of marine-terminating glaciers. We derive the linear relation between δD and δR for 8 major GrIS DS and calculate the regional annual δD from 1960 to 2013 using this linear relation.

Hereafter, the regional cumulative discharge anomaly (δD), which is derived from the RACMO2 runoff, is denoted as D^R, while D^{D-08} and D^{D-14} refer to δD based on Rignot-08 and Enderlin-14, respectively. We compare D^R, D^{D-08} and D^{D-14} in Fig. 2 for the time interval 2000 to 2007, which is common to both D^{D-08} and D^{D-14}. In DS7, where $R^2 = 0.94$, D^{D-08} and D^{D-14} are similar, $-20.1 \pm 1.9\,\mathrm{Gt\,yr^{-1}}$ and $-17.6 \pm 2.2\,\mathrm{Gt\,yr^{-1}}$ respectively. However, in the same region, D^R is $-8.9 \pm 4.7\,\mathrm{Gt\,yr^{-1}}$. The difference between the runoff-derived and flux gate D estimates may indicate that the reference D_0 for this region should be $\sim$-9 $\mathrm{Gt\,yr^{-1}}$ lower than D_0 estimated by Rignot-08. A similar difference can be seen in DS4 where we obtain $36.2 \pm 2.5\,\mathrm{Gt\,yr^{-1}}$ for D^{D-14} and $37.9 \pm 2.8\,\mathrm{Gt\,yr^{-1}}$ for D^{D-08}, but D^R is $8.4 \pm 3.3\,\mathrm{Gt\,yr^{-1}}$. However, in DS4, D^R is probably not reliable as the runoff-to-discharge correlation is weak in this region ($R^2 = 0.38$). For the entire GrIS, the reference D_0 is 427 ± 30 Gt for D^{D-08}, and 414 ± 44 Gt for D^{D-14}. When applying the runoff based interpolated D_0 only for DS1, DS3, DS7 and DS8, with the rest of DSs using D^{D-14}, D_0 becomes 410 ± 37 Gt, i.e. in that case they agree within the uncertainties.

In order to evaluate the SMB_0 and D_0 used in this study, we compare the IOM regional mass balance in 8 major basins (interior and coastal regions are combined), and apply both Eqs. (5) and (6). The latter equation relies on the determination of the SMB_0 and D_0 while Eq. (5) does not, so the comparison can provide an indication about the reliability of the SMB_0 and D_0 for some basins. For the application of Eq. (6) we use two

TCD
9, 4661–4699, 2015

methods. Method 2 uses D^{D-14} while method 3 uses D^{R} in DS 1, 3, 7 and 8. As can be seen in Fig. 3, the three methods agree for the whole GrIS and for most of the basins within the uncertainties. In DS 4, 7 and 8, however, methods 1 and 2 are significantly different, which may be caused by underestimated cumulative errors in Eq. (5) or less accurate reference SMB_0 and D_0. This is further discussed in Sect. 4.

2.4 The IOM based simulation

The GrIS monthly mass balance simulations that will be used in Sect. 3 are based on the IOM solutions. We interpolate SMB and D onto a gridded map of EWH with a resolution of 1 arc degree for the GrIS and surrounding areas. To account for leakage from outside the GrIS, as occurs in GRACE, we apply the annual mass changes estimates from Schrama et al. (2014) for all the major glacier areas (GrIS excluded). We convolve the gridded mass distribution over the Earth's surface and obtain the potential coefficients in response to this distribution up to d/o 60. Noise in the monthly GRACE coefficients manifests mainly as north-south stripes in the spatial domain (Swenson and Wahr, 2006). In order to mimic this error in the simulation, we add randomly generated noise as described in Bonin and Chambers (2013) to the potential coefficients

3 GRACE

3.1 Post-processing GRACE data

In this study we use the GRACE release 5 level 2 monthly spherical harmonics coefficients C_{lm} and S_{lm} ("GSM") produced by the University of Texas Center for Space Research (CSR). The time interval is from January 2003 to January 2014 and the maximum spherical harmonic degree $l = 60$. We add C_{10}, C_{11} and S_{11} coefficients (associated with geocenter loading) obtained from GRACE data and independent oceanic and atmospheric models (Swenson et al., 2008). The geopotential flattening coefficient

TCD
9, 4661–4699, 2015

(C_{20}) in GRACE data is less accurate than from the Satellite Laser Ranging (SLR) measurements (Chen et al., 2004), thus we replace this coefficient with the ones from Cheng et al. (2013). The GRACE potential coefficients are averaged between January 2003 and January 2014 and this average field serves as a reference to obtain monthly anomalies ΔC_{lm} and ΔS_{lm}.

GRACE observations of mass change within a sub-region of the GrIS are affected by mass changes in neighbouring areas, a phenomenon known as leakage (Wahr et al., 1998). But GRACE data should also be corrected for known oceanic and atmospheric mass motions, continental hydrology and Glacial Isostatic Adjustment (GIA). The oceanic and atmospheric mass changes are already removed from the coefficients provided by CSR. The Global Land Data Assimilation System (GLDAS) model (Rodell et al., 2004) is employed to simulate the continental hydrology, which is then removed from the GRACE monthly coefficients. Note that permafrost regions are excluded in the GLDAS version 2 1.0 degree monthly data that are obtained from Goddard Earth Sciences Data and Information Services Center.

The GIA effect in the GRACE data for the GrIS is compensated via the model output of Paulson et al., (2007), which is based on an the ICE-5G ice loading history and the VM2 Earth model (Peltier 2004). Hereafter we refer to this model by Paulson-07. In addition to this model, 11 alternative GIA models are employed based on different ice history and viscosity models to determine the uncertainty in the GIA correction. For instance, the models of van der Wal et al., (2013) include 3D changes in viscosity and the model of Simpson et al. (2009) uses a different ice loading history, see the summary of the GIA models used in this study in Table A3. An isotropic Gaussian filter is employed to reduce the noise in GRACE data (Wahr et al. 1998), with a half width of $r_{1/2} = 300$ km.

3.2 Inversion of the regional mass balance

To estimate the regional mass balance in separate GrIS basins, we apply a constrained least-squares inversion approach (Bonin and Chambers, 2013; Schrama and Wouters,

TCD
9, 4661–4699, 2015

2011).

$$\hat{x} = (\boldsymbol{H}^T\mathbf{H} + \mathbf{P}^{-1})\boldsymbol{H}^T\boldsymbol{y}. \quad (9)$$

The vector $\boldsymbol{y}$ contains the monthly GRACE data. To compute the influence functions in the design matrix $\mathbf{H}$ we assume a layer of water with unit height uniformly distributed over the mascon, then express the mass change in spherical harmonic coefficients up to d / o 60, similar to the GRACE data. The vector $\hat{x}$ represents the scale factors for the unit mass changes in each basin that we aim to find. $\mathbf{P}$ is the covariance matrix of the mass changes in each mascon. When assuming that the mass changes in each equally weighted mascon are independent then $\mathbf{P} = \lambda\mathbf{I}$, with λ the prior variance of the regional mass changes. In our previous study, we demonstrated that three different prior variances for the GrIS regions below and above 2000 m, as well as for the surrounding Arctic regions respectively improved the recovery of regional mass changes (Xu et al. 2015). Using a simulation model based on the IOM (see Sect. 2.4) optimal regional constraints were determined, i.e. for coastal mascons $\lambda_a = 13\,\mathrm{m}^2$, for inland mascons $\lambda_b = 0.1\,\mathrm{m}^2$ and for the nearby surrounding EBIS regions (Ellesmere island, Baffin island, Iceland and Svalbard) regions $\lambda_{\mathrm{EBIS}} = 11\,\mathrm{m}^2$.

3.3 Approximation errors

In the solution of $\hat{x}$, two types of errors occur: (a) systematic errors are caused by measurement errors propagated through the least-squares approach and (b) the additional error that is introduced when applying Eq. (9). For the type (b) error, Bonin and Chamber (2013) show that Eq. (9) leaves a noticeable difference between the approximation $\hat{x}$ and the "truth" (a GrIS mass changes simulation), in particular in GrIS sub-regions, which they categorize as a uncertainty which we recognize as an error source. Hereafter the type (b) error is denoted as "approximation error" or ε. We estimate ε by using simulations of GrIS as $\boldsymbol{x}$, following Bonin and Chambers (2013) so that the approximation error becomes $\varepsilon = \boldsymbol{x} - \hat{x}$. The simulated regional mass changes on the mascons

TCD
9, 4661–4699, 2015

are $\boldsymbol{x} = [x_1, x_2 x_3, \ldots, x_n]$, where n is the total number of mascons. We will show that there is a relation between $\hat{x}$ and $\boldsymbol{x}$, which can be used to correct for the approximation errors.

The simulation model $\boldsymbol{y} = f(\theta\lambda)$ is based on 10 years (2003 to 2012) of mass changes obtained from the IOM (see Section 2.3), with errors written as $\sigma(\theta\lambda)$. We employ a Monte-Carlo approach to simulate a sample of 1000 randomly distributed observations, according to $\boldsymbol{y}'_i = y + k_i\sigma$ with $\boldsymbol{k}_i = k_i(\theta\lambda)$ a vector of random scaling factors varying from -1 to 1, and index i running from 1 to 1000. Hereby it is important to note that we assume that measurement errors do not exist (i.e. the simulation model is assumed to be reality); in addition we assume that the generated samples in the simulation (σ) are normally distributed.

Next we apply Eq. (9) to yield approximated regional mass changes $\hat{x} = [\hat{x}_i]$, in which i is the index of the mascons (see Fig. 1). From the simulation we can derive the real regional mass change rate $\boldsymbol{x} = [x_i]$. As mentioned above, the difference between $\hat{x}$ and $\boldsymbol{x}$ equals the approximation error. In Fig. 4 we show that the x_i are linearly correlated with $\hat{x}_i$. By applying this correlation to the approximations derived from GRACE data, one can reduce the approximation errors in the GRACE based regional mass balance approximations.

The simulated trend in regional mass changes $\boldsymbol{x}'$ and the corresponding approximation $\hat{x}'$ are shown in Fig. 4. It can be noticed that the approximations are strongly correlated with the simulation in the coastal regions over time and with an average correlation coefficient $R^2 = 0.9$. This means that the approximated regional solutions are close to the simulation. The correlation in region DS1a is weaker (~ 0.6), which suggests that the approximation for region DS1a is influenced more by mass changes in neighbouring regions such as region DS8a. In the simulation the inter-region correlation between DS1a and DS8a is ~ -0.1, while in the approximations, the correlation rises to ~ -0.5. By comparison, another neighbour of DS8a, DS7a, has a very weak inter-region correlation with DS8a both in the simulation and in the approximation (~ 0.04). The inter-region correlation errors are systematic due to the least-squares in-

TCD
9, 4661–4699, 2015

version (Bonin and Chambers, 2013; Schrama and Wouters, 2011). Previous work shows that the regional approximation errors can be reduced when specifying constraints for the GrIS coastal and inland regions, but within the coastal region all the sub-DSs are constrained by the same prior variance in this study, thus the increase in correlation between DS1a and DS8a remains.

For the coastal regions, there is a linear relationship between the simulations $\boldsymbol{x}$ and the approximation $\hat{x}$, as can be seen in Fig. 4. We fit this relationship by $\boldsymbol{x} = \alpha_1 \hat{x} + \alpha_0$, with a summary of α_1 and α_0 given in Table A1. The linear relationship between the simulated and the approximated regional mass changes rates is found to be stable; even when the simulation uncertainties are multiplied with a factor or 5 (light green marks in Fig. 4), the average regression parameters ($\alpha_1$and α_0) vary by less than $\sim 1\,\%$ for the coastal mascons. Therefore it is reasonable to assume α_1 and α_0 should also reflect the relationship between the reality and the approximation, as derived from GRACE observations. When the vector of observations $\boldsymbol{y}$ becomes the GRACE observations, by applying the linear relationship to the corresponding approximation $\hat{x}$ can be improved. We will show that this correction yields better agreement between GRACE and the IOM in Sect. 4.

Contrary to the coastal regions, the linear relation between $\mathbf{x}$ and $\hat{x}$ is weak in the interior regions, where the mean correlation coefficient is ~ 0.2. This may be because interior regions show smaller mass change rates than the coastal regions. For simulations created within a 1σ range, the highest correlation coefficient is only 0.47 for DS7b. The strong constraint used for these regions, i.e. a prior variance of 0.1 m^2, may cause the approximation to be more determined by this constraint than the simulation. However, if we apply a weaker constraint, i.e. $\lambda = 10^6$, the correlation coefficients between $\boldsymbol{x}$ and $\hat{x}$ in these regions remain below 0.5. This means that correcting the approximation errors using the same method as for the coastal regions may create larger uncertainties. Following Bonin and Chambers (2014), we choose to include the approximation errors in the uncertainties but only for the interior regions. The uncertainties are shown in table A1.

TCD
9, 4661–4699, 2015

4 Cross-validation

We compared the regional mass changing rate from GRACE with the IOM (Fig. 5) before and after applying the approximation error correction to GRACE and with different discharge estimations implemented by the IOM, separately for coastal and interior regions. For the coastal regions, we find that the correction of the approximation errors in the GRACE solutions adjusts the mass distributions between adjacent mascons. For instance, the corrected mass loss rate in DS3a increases by 10 Gt yr^{-1} while it reduces the mass loss rate in the adjacent region DS 4a by 15 Gt yr^{-1}. In mascon DS5a, DS6a and DS7a, the combined mass change rate is -107 ± 8 Gt yr^{-1} before correcting and -106 ± 8 Gt yr^{-1} after correcting for regional approximation errors. In mascon DS6a correcting for the approximation error causes a mass loss increase of 13 Gt yr^{-1}.

In the IOM used in the comparison, we only consider TMB in order to reduce the influence of the individual uncertainties in SMB and D. We obtain two IOM solutions, using the reference D_0 by Rignot-08 (method 2) and the interpolated discharges based on RACMO2 runoff (method 3). In mascon DS1a and DS3a, we obtain lower discharge changes rate from method 3 than from method 2. In mascon DS7a, which includes Jakobshavn glacier, method 3 results in smaller mass changes than method 2.

Figure 5 shows that agreement between GRACE and IOM improves after correcting the GRACE approximation errors and applying the runoff based discharge estimations in mascon DS3a, DS5a, DS6a and DS7a. The difference between GRACE and IOM estimates is also reduced in DS1a and DS2a, where the remaining difference falls within the uncertainty margins. The corrected GRACE solution in DS4a is only ~ 3 Gt yr^{-1} lower than the IOM solution while it was 10 Gt yr^{-1} higher before correcting the approximation error. However, regardless of correcting the approximation errors, the GRACE inferred regional mass balance agrees with IOM mass balance in DS4a due to the large uncertainties in the GRACE solution and the RACMO2 model there, i.e. ± 17 Gt yr^{-1} (see table A2). From Fig. 5 we can also make some inferences about

TCD
9, 4661–4699, 2015

the effect of using different methods to estimate reference discharge. Only in mascon DS 8a, IOM and GRACE do not agree within the uncertainties.

For the regions above 2000 m altitude, GRACE inferred regional mass change rates agree with the RACMO2 SMB estimations within uncertainties (see Fig. 5). A noticeable mass increase appears in both GRACE and IOM solutions in mascon 2b (northeast interior). A second observation is that in the IOM, the runoff dominates the regional mass balance on the edge of the southern GrIS interior resulting in mass loss of $-8\,\mathrm{Gt\,yr^{-1}}$. The overall IOM uncertainties in the coastal regions are mainly influenced by the uncertainties in SMB and D estimates, meanwhile applying F^{2000} assumptions contributes additional uncertainties in the GrIS interior regions. In the GRACE solution, the uncertainties are due to the errors in the GRACE coefficients which is not dependent on the altitude, therefore the uncertainty level is similar to the coastal regions.

We also compare our GRACE and IOM solutions to 1) GRACE 2) IOM 3) ICEsat altimetry estimates, as shown in Table 1. All listed GRACE solutions agree within uncertainty levels in DS1, DS2, DS3, DS5 and DS8. In-line with some of the referenced studies, we combine DS6 and DS7. We find a larger rate of mass loss in this area compared to other studies (i.e. $-87 \pm 10\,\mathrm{Gt\,yr^{-1}}$) because a longer time interval is considered in this study and mass loss accelerates by $\sim -16\,\mathrm{Gt\,yr^{2}}$ over the entire period according to our solution. After accounting for this acceleration, all GRACE solutions become similar in this combined region.

In the southeast region DS 4, the regional acceleration of mass loss is negligible ($\sim -0.1\,\mathrm{Gt\,yr^{2}}$). When comparing different GRACE solution, the mass loss rate in DS4 ranges from $-28 \pm 7\,\mathrm{Gt\,yr^{-1}}$ to $-51 \pm 6\,\mathrm{Gt\,yr^{-1}}$. It suggests that a large approximation error, which is associated with different approximation approaches, is likely present in this region in the GRACE solution. As shown in Fig. 5, the regional mass change is reduced by 29 % in this region after applying the correction.

The IOM is also relatively uncertain in DS4 (Sasgen et al., 2012). Even if the mass changes rates are very different between GRACE and IOM in this region, agreement is obtained within the large uncertainties. For ICEsat-based mass loss estimates, the

TCD
9, 4661–4699, 2015

retrieved long-term mass loss can be very different, e.g. $-75 \pm 2\,\mathrm{Gt\,yr^{-1}}$ by Zwally et al. (2011) compared to $-40 \pm 18\,\mathrm{Gt\,yr^{-1}}$ by Sørensen et al. (2011). This may be explained by the complicated regional ice surface geometry in the coastal areas (Zwally et al., 2011).

Another area where GRACE and IOM do not agree is the northwest (region DS8). In this region, mass loss is accelerating by $-3 \pm 0.4\,\mathrm{Gt\,yr^{-2}}$ and $-5 \pm 1\,\mathrm{Gt\,yr^{-2}}$ according to our GRACE solution and IOM solution respectively. If we extend the time interval to 2013, we find that GRACE and ICEsat solutions suggest a similar mass loss rate (see Table 1). Moreover, if we determine the mass change rates for the time interval from 2007–2011, the rate is $-57 \pm 6\,\mathrm{Gt\,yr^{-1}}$ (GRACE) and $-49 \pm 11\,\mathrm{Gt\,yr^{-1}}$ (IOM), and both agree with the rate from Andersen et al. (2015). We have reduced the approximation error in the GRACE solution for this region, although by a small amount ($-2.3\,\mathrm{Gt\,yr^{-1}}$).

There is another way to judge whether approximation errors exist in GRACE. When the approximation errors exist for one region, the error is likely of similar magnitude but of opposite sign in neighbouring regions, which we refer to as negative correlation errors (Xu et al. 2015). In this study, the adjacent regions of DS8 are DS1, DS7 and Ellesmere Island and in all three neighbour regions, the mass changes rate between GRACE and IOM solutions are similar, see Fig. 5. This suggests that the difference of the regional mass changes in DS8 is not due to the approximation error in the GRACE solution. The uncertainties of the GIA effect are included as part of the uncertainties of the GRACE solution for this region as well (see Table A3), but adding these still cannot bridge the gap between GRACE and IOM. The ICEsat-based mass change estimate by Kjeldsen et al. (2013) yields a mass loss rates of $55 \pm 8.4\,\mathrm{Gt\,yr^{-1}}$ from 2003 to 2010, which is consistent with the GRACE solution in this study. All evidence combined indicates that the IOM method underestimates the mass loss rate in this basin by $\sim$ -15 $\mathrm{Gt\,yr^{-1}}$. In Sasgen et al. (2012), the discharge estimations from Rignot-08 are used, in which a portion of DS8 was un-surveyed, to which they ascribed the difference between GRACE and IOM ($24 \pm 13\,\mathrm{Gt\,yr^{-1}}$). In this study, the discharge estimation from Enderlin et al. (2014) covers the entire glacier area in this region, but only for the years

TCD
9, 4661–4699, 2015

after 2000. Therefore, despite observations of relatively stable terminus positions for the majority of the marine-terminating glaciers in northwest Greenland between 1985–2000 (Howat and Eddy, 2011), we hypothesize that the estimated reference discharge over-estimates the regional D_0. Deriving D_0 from $D - 14$ involved the assumption that D from 1990 to 2000 follows Rignot-08, which contains high regional uncertainties. On the other hand, if we use the runoff-based estimate of D_0, uncertainties are influenced by the uncertainty of the RACMO2 model. The SMB inter-comparison study of Vernon et al. (2013) shows that the 1961-1990 reference SMB_0 of RACMO2 model is larger than some other SMB models, e.g. MAR or PMM5. It is interesting to see that when the cumulative TMB is calculated independently from the reference SMB_0 and D_0 (using Eq (5), method 1) the mass changes rate becomes similar to the GRACE mass balance in this region. This indicates that modelled SMB (as well as SMB_0) could have uncertainties that are larger than 18 %.

5 Conclusions

In this study, we implement a simulation of GrIS mass changes and show that the approximation errors caused by the Least Squares inversion approach can be quantified and furthermore be reduced in the GRACE solution. For using the IOM, we apply an improved reference discharge estimate that can better agree with other independent estimates. We show that the regional differences between our GRACE and IOM solutions are reduced and agree within the calculated confidence intervals. This is confirmed by an inter-comparison with ICEsat based regional mass change rates. In the southeast, the corrections for the approximation errors in GRACE are especially important. We find that the IOM solutions underestimate mass loss in the northwest compared to GRACE and ICESAT solutions, which we attribute to incorrect estimates in reference D and/or SMB used to construct the IOM estimates. For the whole GrIS and considering the early half of the comparison time window, we find a $208 \pm 18\,\mathrm{Gt\,yr^{-1}}$ mass loss rate for the period 2003 to 2008 from the GRACE solution, while the IOM solution shows

TCD
9, 4661–4699, 2015

a mass loss rate of $195 \pm 25\,\mathrm{Gt\,yr^{-1}}$. The loss rates increase by ~67 % and ~85 % in 2009–2014 in the GRACE and IOM solutions, respectively. The 10-year acceleration in the GRACE data is $-25 \pm 8\,\mathrm{Gt\,yr^{-2}}$, consistent with the IOM solution, $-26 \pm 12\,\mathrm{Gt\,yr^{-2}}$.

Appendix A: Reference discharge based on the pre-1960 discharge estimations

The GrIS ice discharge D was distributed into 34 glaciers by Rignot et al. (2008), denoted by D-08. The reference discharge D_0-08 is considered equivalent to the discharge estimation for the year of 1996. We define the reference discharge in 1996 and 2000 as D_0-08 and D_{2000}-08, respectively. The deviations between D_0-08 and D_{2000}-08 are due to the discharge changes in late 1990s (Enderlin et al., 2014). Similarly, we define Enderlin-14 as D-14, with the time series starting from the year of 2000 (D_{2000}-14). In order to estimate the reference discharge D_0-14, we find scaling factors between D_0-08 and D_{2000}-08 and scale the D_{2000}-14 to yield the estimation of D_0-14. We estimate the uncertainties of estimated D_0-14 via 500 pairs of randomly generated $\widetilde{D}_0$-08, $\widetilde{D}_{2000}$-08 and $\widetilde{D}_{2000}$-14, following from the normal distribution N (D, σ_D), in which σ_D is the error in the discharge estimations. For the entire GrIS, we find that the interpolated $\mathrm{D14}_0 = 413.8 \pm 31.6$ Gt, similar to previous studies (Sasgen et al., 2012; van den Broeke et al., 2009).

A1 Approximation error correction

In order to determine the linear relationship between the simulated regional mass balances with the associated approximations after applying the Least Squares inversion, the linear fitting parameters k_0 and k_1 are calculated for different simulation error levels, the values of which are shown in Table A1. The values of k_0 and k_1 and their uncertainties vary slightly in all coastal regions. In order to determine one value for k_0 and k_1, we assume the k_0 and k_1 follow the normal distribution in each region and draw 1000 random samples for each error level. Then we combine all the samples and fit into

TCD
9, 4661–4699, 2015

another normal distribution, from which the k_0 and k_1 are determined for each region (see the Table A1).

A2 Fitting the long-term regional mass changes rate

$$\boldsymbol{y} = a_0 + a_1\hat{x} + a_2\hat{x}^2 + a_3\cos(\omega\hat{x}) + a_4\sin(\omega\hat{x}),$$

where $= \frac{2\pi n}{12}$, $n = 13$ and $\hat{x} = \boldsymbol{x} - \bar{x}$.

A3 Uncertainty estimations

A summary of the uncertainties in the regional mass balance (linear trend) is shown in Table A2. In our GRACE inferred mass balance, the uncertainties are associated with (1a) the standard deviations of the CSR RL05 GRACE spherical harmonics coefficients (including the standard deviations of the external degree $l = 1$ and 2 coefficients), (2a) the variations of the regional mass changes due to different GIA models and (3a) the uncertainties due to the corrections of the systematic error in the least-squares inversion solutions. The uncertainties of the IOM inferred mass balance consist of the uncertainties of the 1960–1990 reference in SMB_0 and in D_0 and 2b) the systematic error in the SMB (RACMO2) and 2c) the errors in the yearly D estimations (Enderlin, 2014; Rignot, 2008).

A4 Selection of the GIA model for GrIS regions

We apply the GIA correction to the GRACE data using 11 different GIA models before estimating the associated regional mass changes in 20 GrIS and surrounding Arctic regions (see the mascon definition in Sect. 3). By comparing with one without applying GIA correction, we assume the differences are the regional GIA effects. In addition to Paulson-07 GIA model, we use a GIA model with lateral changes in viscosity and the ICE-5G loading history (van der Wal et al. 2013).

TCD
9, 4661–4699, 2015

Moreover, we use 8 different GIA models based on the ice history model from Simpson et al. (2009), provided by Glenn Milne within the scope of the IMBIE project. The upper mantle viscosity ranges from 0.3×10^{21} to 1×10^{21} Pa s and the lower mantle viscosity ranges from 1×10^{21} to 10×10^{21} Pa s. The thickness of the lithosphere is assumed to be 96 km or 120 km.

In Table A3, the GIA related mass changes can vary from $-7\,\mathrm{Gt\,yr^{-1}}$ to $10\,\mathrm{Gt\,yr^{-1}}$ for the entire GrIS. A positive GIA effect appears in the northern GrIS while in the south and southwest GrIS, (DS 5a to DS 7a) negative GIA signals prevail.

In order to quantify the uncertainties of the regional GIA in the Paulson-07, since it is the GIA model we used to derive our GRACE solution, we estimate the standard deviation of all models with respect to Paulson-07. The uncertainties are summarized in Table A2.

Acknowledgements. This research is funded by means of scholarship GO-AO/27 provided by the Netherlands Organization of Scientific Research, NWO. We are grateful to Ian Joughin for the suggestions of estimating the ice flux at high elevation. Furthermore the authors acknowledge thoughtful comments by Etienne Berthier of this manuscript.

References

Andersen, M. L., Stenseng, L., Skourup, H., Colgan, W., Khan, S. A., Kristensen, S. S., Andersen, S. B., Box, J. E., Ahlstrøm, A. P., Fettweis, X., and Forsberg, R.: Basin-scale partitioning of Greenland ice sheet mass balance components (2007–2011), Earth Planet. Sci. Lett., 409, 89-95, 2015.

Bales, R. C., Guo, Q., Shen, D., McConnell, J. R., Du, G., Burkhart, J. F., Spikes, V. B., Hanna, E., and Cappelen, J.: Annual accumulation for Greenland updated using ice core data developed during 2000–2006 and analysis of daily coastal meteorological data, J. Geophys. Res.-Atmos., 114, 2009.

Barletta, V. R., Sørensen, L. S., and Forsberg, R.: Scatter of mass changes estimates at basin scale for Greenland and Antarctica, The Cryosphere, 7, 1411-1432, 2013, http://www.the-cryosphere-discuss.net/7/1411/2013/.

TCD
9, 4661–4699, 2015

Bonin, J. and Chambers, D.: Uncertainty estimates of a GRACE inversion modelling technique over Greenland using a simulation, Geophys. J. Int., 194, 212—29, 2013.
Chen, J., Wilson, C., Tapley, B., and Ries, J.: Low degree gravitational changes from GRACE: Validation and interpretation, Geophys. Res. Lett., 31, 2004.
Cheng, M., Tapley, B. D., and Ries, J. C.: Deceleration in the Earth's oblateness, J. Geophys. Res.-Sol. EA, 118, 740–747, 2013.
Cogley, J. G.: Greenland accumulation: An error model, J. Geophys. Res.-Atmos., 109, 2004.
Colgan, W., Abdalati, W., Citterio, M., Csatho, B., Fettweis, X., Luthcke, S., Moholdt, G., and Stober, M.: Hybrid inventory, gravimetry and altimetry (HIGA) mass balance product for Greenland and the Canadian Arctic, The Cryosphere Discuss., 8, 537–580, doi:10.5194/tcd-8-537-2014, 2014.
Enderlin, E. M., Howat, I. M., Jeong, S., Noh, M. J., Angelen, J. H., and Broeke, M. R.: An improved mass budget for the Greenland ice sheet, Geophys. Res. Lett., 41, 866–872, 2014.
Ettema, J., van den Broeke, M. R., van Meijgaard, E., van de Berg, W. J., Bamber, J. L., Box, J. E., and Bales, R. C.: Higher surface mass balance of the Greenland ice sheet revealed by high-resolution climate modeling, Geophys. Res. Lett., 36, L12501, doi:10.1029/2009GL038110, 2009.
Fettweis, X.: Reconstruction of the 1979–2006 Greenland ice sheet surface mass balance using the regional climate model MAR, The Cryosphere Discuss., 1, 123–168, doi:10.5194/tcd-1-123-2007, 2007.
Gallée, H. and Schayes, G.: Development of a three-dimensional meso-γ primitive equation model: Katabatic winds simulation in the area of Terra Nova Bay, Antarctica, Mon Weather Rev, 122, 671–685, 1994.
Groh, A., Ewert, H., Fritsche, M., Rülke, A., Rosenau, R., Scheinert, M., and Dietrich, R.: Assessing the Current Evolution of the Greenland Ice Sheet by Means of Satellite and Ground-Based Observations, Surv. Geophys, 1–22, 2014.
Hanna, E., Huybrechts, P., Janssens, I., Cappelen, J., Steffen, K., and Stephens, A.: Runoff and mass balance of the Greenland ice sheet: 1958–2003, J. Geophys. Res.-Atmos., 110, D13108, doi:10.1029/2004JD005641, 2005.
Howat, I. M. and Eddy, A.: Multi-decadal retreat of Greenland's marine-terminating glaciers, J Glaciol, 57, 389–396, 2011.

TCD
9, 4661–4699, 2015

Howat, I. M., Ahn, Y., Joughin, I., van den Broeke, M. R., Lenaerts, J., and Smith, B.: Mass balance of Greenland's three largest outlet glaciers, 2000–2010, Geophys. Res. Lett, 38, L12501, doi:10.1029/2011GL047565, 2011.
Johannessen, O. M., Khvorostovsky, K., Miles, M. W., and Bobylev, L. P.: Recent ice-sheet growth in the interior of Greenland, Science, 310, 1013–1016, 2005.
Jürgen, B., Kalyanmoy, D., Kaisa, M., and Roman, S.: Multiobjective Optimization: Interactive and Evolutionary Approaches, ISBN: 978-3-540-88907-6, 2008.
Kjeldsen, K. K., Khan, S. A., Wahr, J., Korsgaard, N. J., Kjær, K. H., Bjørk, A. A., Hurkmans, R., Broeke, M. R., Bamber, J. L., and Angelen, J. H.: Improved ice loss estimate of the northwestern Greenland ice sheet, J. Geophys. Res.-Sol. EA, 118, 698–708, 2013.
Luthcke, S. B., Zwally, H., Abdalati, W., Rowlands, D., Ray, R., Nerem, R., Lemoine, F., McCarthy, J., and Chinn, D.: Recent Greenland ice mass loss by drainage system from satellite gravity observations, Science, 314, 1286–1289, 2006.
Luthcke, S. B., Sabaka, T., Loomis, B., Arendt, A., McCarthy, J., and Camp, J.: Antarctica, Greenland and Gulf of Alaska land-ice evolution from an iterated GRACE global mascon solution, J. Glaciol., 59, 613–631, 2013.
Moon, T., Joughin, I., Smith, B., Broeke, M. R., Berg, W. J., Noël, B., and Usher, M.: Distinct patterns of seasonal Greenland glacier velocity, Geophys. Res. Lett, 41, 7209–7216, 2014.
Ohmura, A. and Reeh, N.: New precipitation and accumulation maps for Greenland, J. Glaciol, 37, 140–148, 1991.
Paulson, A., Zhong, S., and Wahr, J.: Inference of mantle viscosity from GRACE and relative sea level data, Geophys. J. Int., 171, 497–508, 2007.
Peltier, W.: Global glacial isostasy and the surface of the ice-age Earth: the ICE-5G (VM2) model and GRACE, Annu. Rev. Earth Planet. Sci, 32, 111–149, 2004.
Rignot, E. and Kanagaratnam, P.: Changes in the velocity structure of the Greenland Ice Sheet, Science, 311, 986–990, 2006.
Rignot, E., Box, J., Burgess, E., and Hanna, E.: Mass balance of the Greenland ice sheet from 1958 to 2007, Geophys. Res. Lett., 35, L20502, doi:10.1029/2008GL035417, 2008.
Rignot, E., Velicogna, I., van den Broeke, M., Monaghan, A., and Lenaerts, J.: Acceleration of the contribution of the Greenland and Antarctic ice sheets to sea level rise, Geophys. Res. Lett., 38, L05503, doi:10.1029/2011GL046583, 2011.

TCD
9, 4661–4699, 2015

Rodell, M., Houser, P., Jambor, U. e. a., Gottschalck, J., Mitchell, K., Meng, C., Arsenault, K., Cosgrove, B., Radakovich, J., and Bosilovich, M.: The global land data assimilation system, B. Am. Meteor. Soc., 85, 381–394, 2004.

Sasgen, I., Martinec, Z., and Bamber, J.: Combined GRACE and InSAR estimate of West Antarctic ice mass loss, J. Geophys. Res.-Earth, 115, F04010, doi:10.1029/2009JF001525, 2010.

Sasgen, I., van den Broeke, M., Bamber, J. L., Rignot, E., Sørensen, L. S., Wouters, B., Martinec, Z., Velicogna, I., and Simonsen, S. B.: Timing and origin of recent regional ice-mass loss in Greenland, Earth Planet. Sci. Lett., 333, 293–303, 2012.

Schrama, E. J. and Wouters, B.: Revisiting Greenland ice sheet mass loss observed by GRACE, J. Geophys. Res.-Sol. EA, 116, 377–385, doi:10.1007/s10712-011-9113-7, 2011.

Schrama, E. J., Wouters, B., and Rietbroek, R.: A mascon approach to assess ice sheet and glacier mass balances and their uncertainties from GRACE data, J. Geophys. Res.-Sol. EA, 2014.

Shepherd, A., Ivins, E. R., Geruo, A., Barletta, V. R., Bentley, M. J., Bettadpur, S., Briggs, K. H., Bromwich, D. H., Forsberg, R., and Galin, N.: A reconciled estimate of ice-sheet mass balance, Science, 338, 1183–1189, 2012.

Simpson, M. J., Milne, G. A., Huybrechts, P., and Long, A. J.: Calibrating a glaciological model of the Greenland ice sheet from the Last Glacial Maximum to present-day using field observations of relative sea level and ice extent, Quat. Sci. Rev., 28, 1631–1657, 2009.

Sørensen, L. S., Simonsen, S. B., Nielsen, K., Lucas-Picher, P., Spada, G., Adalgeirsdottir, G., Forsberg, R., and Hvidberg, C. S.: Mass balance of the Greenland ice sheet (2003–2008) from ICESat data – the impact of interpolation, sampling and firn density, The Cryosphere, 5, 173–186, doi:10.5194/tc-5-173-2011, 2011.

Swenson, S. and Wahr, J.: Post-processing removal of correlated errors in GRACE data, Geophys. Res. Lett., 33, L08402, doi:10.1029/2005GL025285, 2006.

Swenson, S., Chambers, D., and Wahr, J.: Estimating geocenter variations from a combination of GRACE and ocean model output, J. Geophys. Res.-Sol. EA, 113, 2008.

Swenson, S., Wahr, J., and Milly, P.: Estimated accuracies of regional water storage variations inferred from the Gravity Recovery and Climate Experiment (GRACE), Water Resour. Res., 39, 11.1–11.3, doi:10.1029/2002WR001808, 2003.

Tedesco, M., Fettweis, X., Mote, T., Wahr, J., Alexander, P., Box, J. E., and Wouters, B.: Evidence and analysis of 2012 Greenland records from spaceborne observations, a regional

TCD
9, 4661–4699, 2015

climate model and reanalysis data, The Cryosphere, 7, 615–630, doi:10.5194/tc-7-615-2013, 2013.
Thomas, R., Csatho, B., Davis, C., Kim, C., Krabill, W., Manizade, S., McConnell, J., and Sontag, J.: Mass balance of higher-elevation parts of the Greenland ice sheet, J. Geophys. Res.-Atmos., 106, 33707–33716, 2001.
Tikhonov, A. N.: Regularization of incorrectly posed problems, Soviet Math. Dokl, 1624–1627, 1963.
Uppala, S. M., Kållberg, P., Simmons, A., Andrae, U., Bechtold, V., Fiorino, M., Gibson, J., Haseler, J., Hernandez, A., and Kelly, G.: The ERA-40 re-analysis, Q. J. Roy. Meteor. Soc., 131, 2961–3012, 2005.
van Angelen, J. H., Lenaerts, J. T. M., Lhermitte, S., Fettweis, X., Kuipers Munneke, P., van den Broeke, M. R., van Meijgaard, E., and Smeets, C. J. P. P.: Sensitivity of Greenland Ice Sheet surface mass balance to surface albedo parameterization: a study with a regional climate model, The Cryosphere, 6, 1175–1186, doi:10.5194/tc-6-1175-2012, 2012.
van de Wal, R. S. W., Boot, W., Smeets, C. J. P. P., Snellen, H., van den Broeke, M. R., and Oerlemans, J.: Twenty-one years of mass balance observations along the K-transect, West Greenland, Earth Syst. Sci. Data, 4, 31–35, doi:10.5194/essd-4-31-2012, 2012.
van den Broeke, M., Bamber, J., Ettema, J., Rignot, E., Schrama, E., van de Berg, W. J., van Meijgaard, E., Velicogna, I., and Wouters, B.: Partitioning recent Greenland mass loss, Science, 326, 984–986, 2009.
van der Wal, W., Barnhoorn, A., Stocchi, P., Gradmann, S., Wu, P., Drury, M., and Vermeersen, B.: Glacial isostatic adjustment model with composite 3-D Earth rheology for Fennoscandia, Geophys. J. Int., 194, 61–77, 2013.
Velicogna, I., Sutterley, T., and van den Broeke, M.: Regional acceleration in ice mass loss from Greenland and Antarctica using GRACE time-variable gravity data, Geophys. Res. Lett., 8130–8137, doi:10.1002/2014GL061052, 2014.
Velicogna, I. and Wahr, J.: Time-variable gravity observations of ice sheet mass balance: Precision and limitations of the GRACE satellite data, Geophys. Res. Lett., 40, 3055–3063, 2013.
Vernon, C. L., Bamber, J. L., Box, J. E., van den Broeke, M. R., Fettweis, X., Hanna, E., and Huybrechts, P.: Surface mass balance model intercomparison for the Greenland ice sheet, The Cryosphere, 7, 599–614, doi:10.5194/tc-7-599-2013, 2013.

TCD
9, 4661–4699, 2015

Wahr, J., Molenaar, M., and Bryan, F.: Time variability of the Earth's gravity field: Hydrological and oceanic effects and their possible detection using GRACE, J. Geophys. Res., 103, 30205–30230, 1998.
Wouters, B., Bamber, J., van den Broeke, M., Lenaerts, J., and Sasgen, I.: Limits in detecting acceleration of ice sheet mass loss due to climate variability, Nat. Geosci., 6, 613–616, 2013.
Wouters, B., Chambers, D., and Schrama, E.: GRACE observes small-scale mass loss in Greenland, Geophys. Res. Lett., 35, L20501, doi:10.1029/2008GL034816, 2008.
Xu, Z., Schrama, E., and van der Wal, W.: Optimization of regional constraints for estimating the Greenland mass balance with GRACE level-2 data, Geophys. J. Int., 202, 381–393, 2015.
Zwally, H. and Giovinetto, M.: Spatial distribution of net surface mass balance on Greenland, Ann. Glaciol., 31, 126–132, 2000.
Zwally, H., Schutz, B., Abdalati, W., Abshire, J., Bentley, C., Brenner, A., Bufton, J., Dezio, J., Hancock, D., and Harding, D.: ICESat's laser measurements of polar ice, atmosphere, ocean, and land, J. Geodyn., 34, 405–445, 2002.
Zwally, H. J., Giovinetto, M. B., Li, J., Cornejo, H. G., Beckley, M. A., Brenner, A. C., Saba, J. L., and Yi, D.: Mass changes of the Greenland and Antarctic ice sheets and shelves and contributions to sea-level rise: 1992–2002, J. Glaciol., 51, 509–527, 2005.
Zwally, H. J., Jun, L., Brenner, A. C., Beckley, M., Cornejo, H. G., Dimarzio, J., Giovinetto, M. B., Neumann, T. A., Robbins, J., and Saba, J. L.: Greenland ice sheet mass balance: distribution of increased mass loss with climate warming; 200307 versus 19922002, J. Glaciol., 57, 88–102, 2011.
Zwally, H. J., Giovinetto, M. B., Beckley, M. A., and Saba, J. L.: http://icesat4.gsfc.nasa.gov/cryo_data/ant_grn_drainage_systems.php (last access: last access: 2 September 2015), 2012.

TCD
9, 4661–4699, 2015

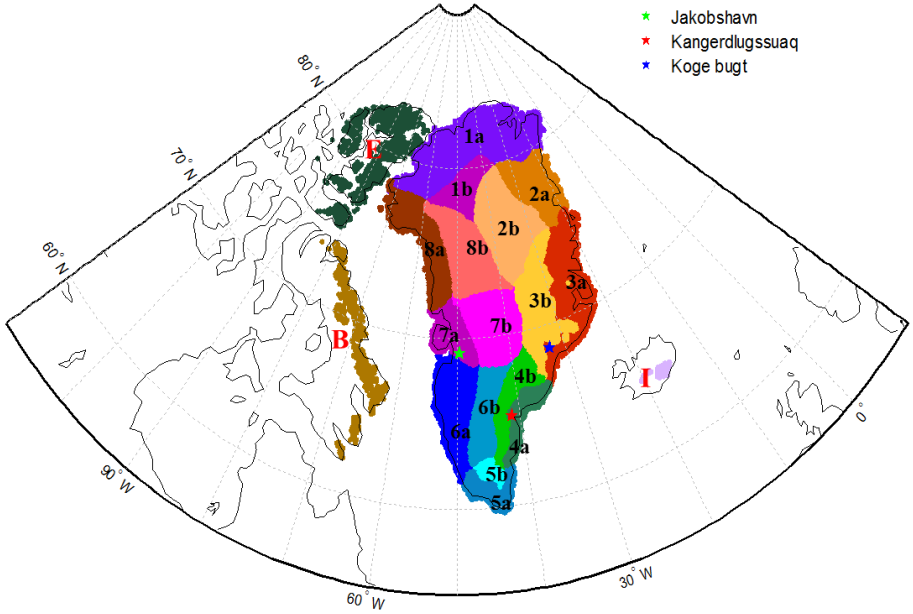

Figure 1. The GrIS mascon layout, based on the basin definition by Zwally (2012). The mascon with the same digits refer to a region belonging to the same drainage system. The characters "a" and "b" indicate the GrIS margin (< 2000 m) and GrIS interior (≥ 2000 m), respectively. There are 16 GrIS mascons and 4 neighbouring Arctic mascons. The location of the three largest discharge outlets are marked with a star, i.e. Jakobshavn (green), Kangerdlugssuaq (red) and Koge Bugt (blue) glaciers. The glacier area is defined in the RACMO2 model.

TCD
9, 4661–4699, 2015

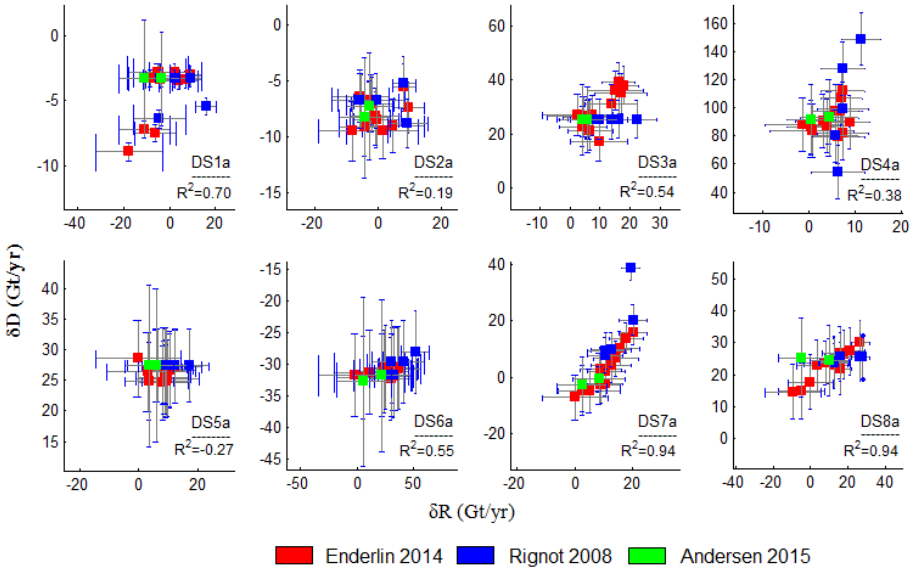

Figure 2. Correlation between the anomaly of the discharge δD with respect to a reference SMB (y axis) and the 4-year averaging runoff δR (x axis) in GrIS regions. The symbols with different colours refer to different estimations of D. The grey bars for both δD and δR indicate the errors. The correlation coefficients R^2 are also shown in each plot.

TCD
9, 4661–4699, 2015

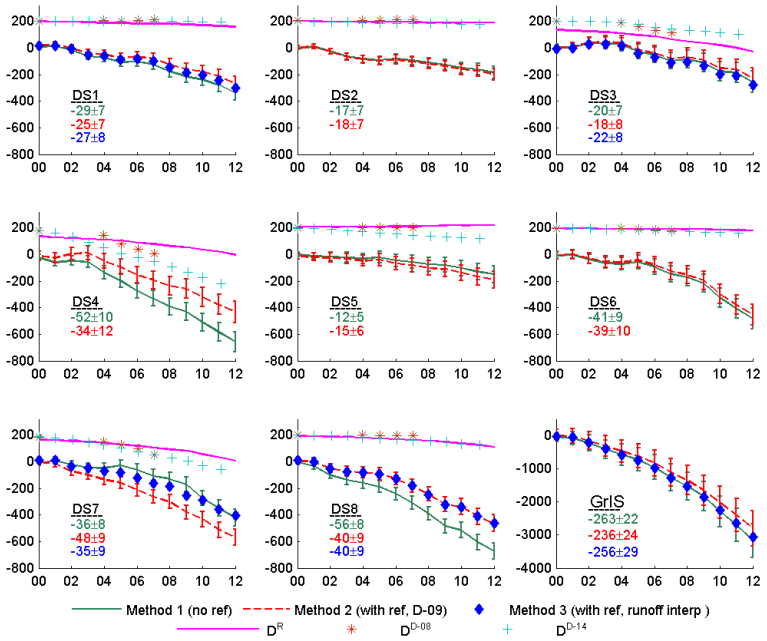

Figure 3. The comparison between cumulative TMB (2000–2012) obtained with three different methods. Method 1, using no reference TMB, is shown with a green curve. The cumulative TMB obtained with a 1960–1990 reference TMB is shown with a red curve (method 2) and blue markers (method 3). Method 2 and Method 3 compute the reference discharge in a different way. In method 2, D0 is based on the estimation from Rignot-08 and for the years after 2000, the estimation from $D-14$ is used (D^{D-14}). Method 3 interpolates the reference discharge using the modelled runoff data (only in DS 1, 3, 7 and 8), denoted as D^R. D^{D-08} refers to the discharge changes by D-08. All the discharges are shifted upward by 200 Gt for visualization purposes. The numbers in each plot indicate the annual TMB change rates with unit Gt yr^{-1}. The x axis shows the last two digits of the years from 2000 to 2012.

TCD
9, 4661–4699, 2015

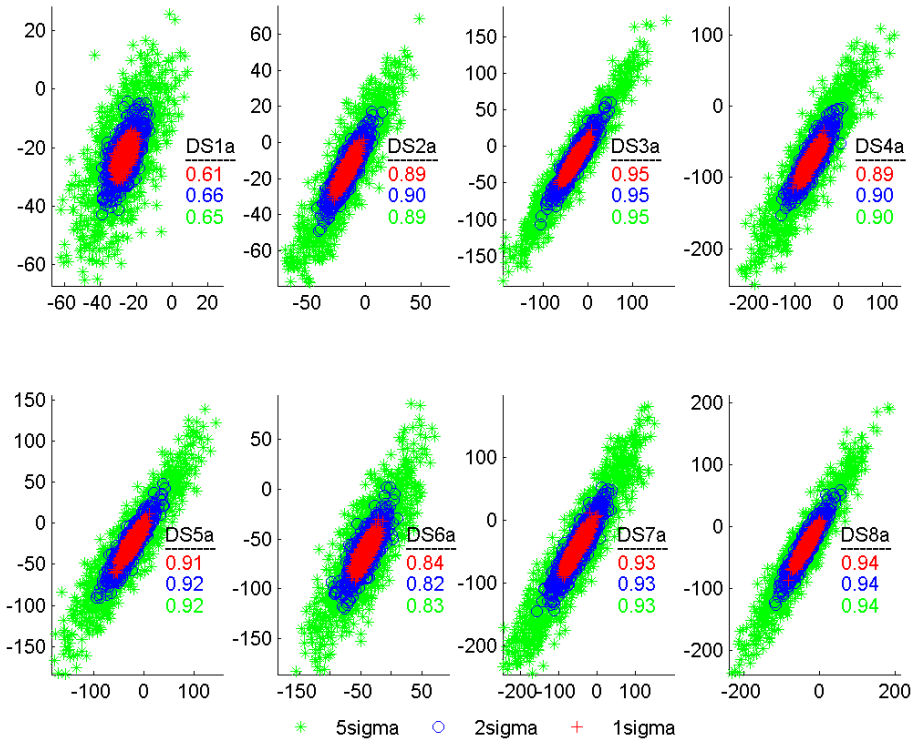

Figure 4. Correlation between the linear trend in the modified simulations x' (y axis) and the corresponding approximation $\hat{x}$ (x axis). The unit is in Gt yr^{-1}. The colours are associated with the changing range of $\hat{x}$ for a standard deviation going from 1σ to 5σ. The numbers refer to the R^2 coefficient for three different

TCD
9, 4661–4699, 2015

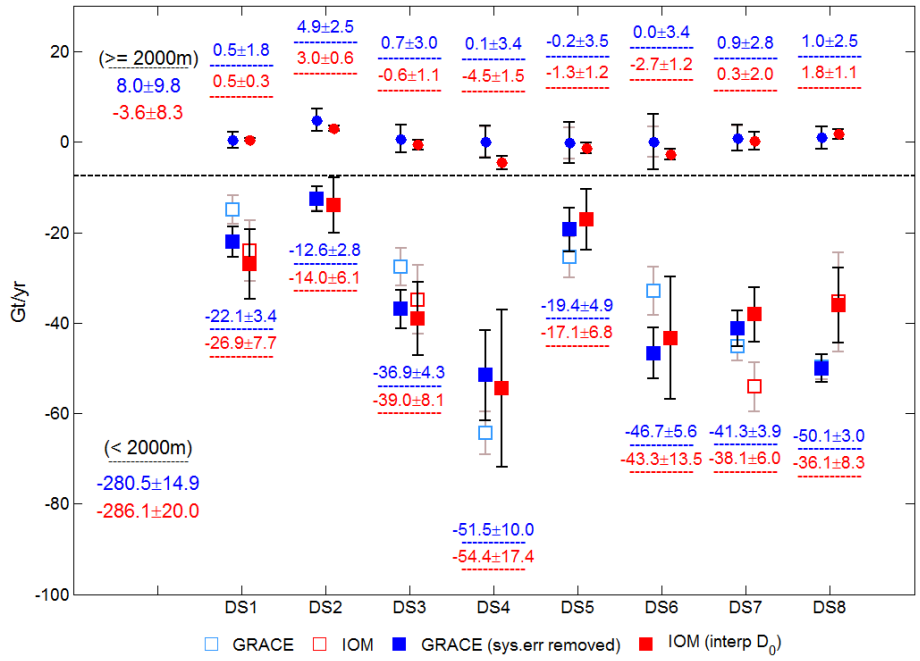

Figure 5. Comparison of the regional mass changes rate between the GRACE solution and the IOM solutions. Each column refers to one complete basin according to Zwally (2012). The regional mass change rates from GRACE before correcting for the approximation error, are represented by the light blue hollow squares; the filled dark blue squares indicate the mass change rates after implementing the correction. The numbers show the mass changes rate in blue and red colour which indicate the GRACE solution and IOM solution respectively. The dashed line separates the solutions from the interior regions (above the dashed line) from the coastal regions (below the dashed line). The error bars are estimated in Appendix A4.

TCD
9, 4661–4699, 2015

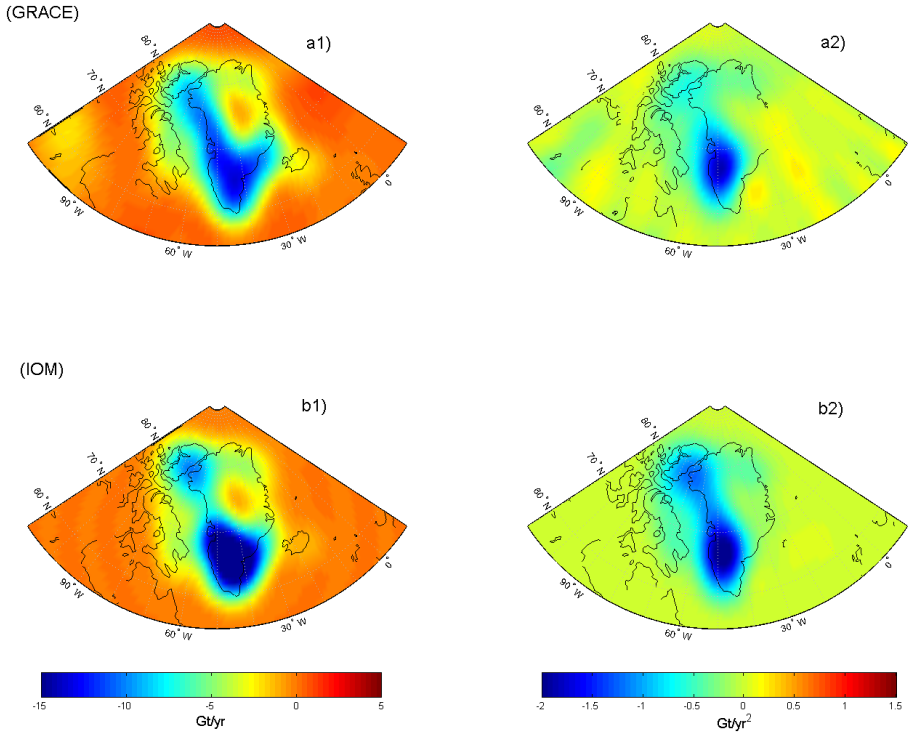

Figure A1. The EWH of the linear trend (a1) and accelerations (a2) in CSR release 5 level 2 GRACE data. The linear trend (b1) and the accelerations (b2) of IOM solution in EWH. The time interval is from Jan 2003 to Jan 2012. The Gaussian filter halfwidth in all plots is $r_{1/2}$ = 300 km

TCD
9, 4661–4699, 2015

Table 1. Linear trends in the mass changes in GrIS regions based on satellite gravity data (GRACE), IOM output and altimetry data (ICEsat). The unit is Gt yr^{-1}. The studies are: Zwally et al. (2011); Sasgen et al. (2012); Barletta et al. (2013); Colgan et al. (2013); Groh et al. (2014); Andersen et al. (2015); Sørensen et al. (2011).

Basin	DS 1	DS 2	DS 3	DS 4	DS 5	DS 6	DS 7	DS 8
	GRACE							
This study (2003-2013)	−22 ± 4	−8 ± 4	−36 ± 5	−51 ± 6	−20 ± 6	−47 ± 8	−40 ± 5	−50 ± 4
Colgan (2003–2010)	−21 ± 6	1 ± 6	−47 ± 13	−28 ± 7	−24 ± 4	−33 ± 7	−23 ± 9	−42 ± 12
Sasgen (2003–2010)	−16 ± 5	−12 ± 5	−38 ± 6	−42 ± 6	−24 ± 6	−56 ± 7		−53 ± 7
Barletta (2003-2012	−17 ± 2	−12 ± 2	−36 ± 4	−35 ± 3	−23 ± 2	−66 ± 4		−44 ± 4
	IOM							
This study (2003–2013)	−26 ± 8	−10 ± 6	−39 ± 8	−59 ± 18	−18 ± 7	−46 ± 14	−38 ± 6	−35 ± 8
Andersen (2007–2011)	−17 ± 5	−13 ± 6		−38 ± 29	−20 ± 9	−53 ± 13	−53 ± 17	−58 ± 14
Sasgen (2003-2010)	−20 ± 4	−16 ± 5	−31 ± 8	−66 ± 21	−20 ± 7	−66 ± 20		−26 ± 12
	ICESat							
Zwally −11 (2003–2007)	1 ± 0	13 ± 0	−51 ± 1	−75 ± 2	−10 ± 0	−4 ± 0	−14 ± 0	−33 ± 1
Sørensen (2003–2009)	−16 ± 1	−16 ± 3	−40 ± 18	−43 ± 11	−26 ± 5	−51 ± 7		−53 ± 3

TCD
9, 4661–4699, 2015

Table A1. The linear fit parameters k_0 and k_1 describing the relationship between the regional simulated mass balance and the approximations obtained after the inversion procedure as applied to GRACE data of the coastal regions. For the interior GrIS regions, we show the approximation errors as additional uncertainties.

mascon (< 2000m)	DS 1a	DS 2a	DS 3a	DS 4a	DS 5a	DS 6a	DS 7a	DS 8a
k_0	-10.93 ± 1.46	-0.64 ± 0.54	6.82 ± 1.47	-14.90 ± 1.54	-1.86 ± 1.61	-17.15 ± 1.54	2.54 ± 2.23	0.28 ± 1.02
k_1	0.85 ± 0.03	1.02 ± 0.02	0.95 ± 0.01	0.96 ± 0.02	0.90 ± 0.01	0.90 ± 0.02	0.97 ± 0.01	1.00 ± 0.01
mascon (> = 2000 m)	DS 1b	DS 2b	DS 3b	DS 4b	DS 5b	DS 6b	DS 7b	DS 8b
uncertainty (Gt yr^{-1})	0.28	0.35	0.45	0.6	2.88	5.1	0.67	0.65

TCD
9, 4661–4699, 2015

Table A2. The uncertainties associated with the regional mass changes rate. For the GRACE inferred regional solutions, "coef.std" refers to the errors due to the standard deviations in the CSR RL05 spherical coefficients, "GIA" refers to the errors obtained from comparing 11 GIA models. Note that the GIA uncertainties in the interior GrIS are all close to 0 thus they are neglected. In the column with the header "Cor" we show the uncertainties which are caused by the approximation error correction. For SMB and *D* trend estimations, the uncertainties consist of the reference SMB0 and D0 error ("SMB0" and "D0") and the systematic errors in RACMO2 model and in the discharge estimations ("sys"). The column entitled with "Cum. Uncer" refers to uncertainties using the assumptions (1) and (2), see the details in Sect. 3.2. The highlighted columns show the total uncertainties of the linear fit of the GRACE and IOM mass balances.

Mascon	GRACE				RACMO2 (SMB)			Discharge (D)			Cum.Uncer	IOM
	coef.std (1a)	GIA (2a)	Cor (3a)	Total	SMB_0 (1b)	Sys (2b)	Total	D_0 (1c)	Sys (2c)	Total	Apply assum. (1) and (2)	[0cm]SMB-D
DS 1a	1.9	3.9	1.6	3.4	1.9	7.2	7.6	0.8	0	0.8	1.1	7.7
DS 2a	2.1	2.2	0.6	2.8	1.6	5.8	6	1.1	0.3	1.1	2.9	6.8
DS 3a	3.2	3	1.5	4.3	3.6	6.8	7.8	2	1	2.2	2.1	8.4
DS 4a	3.8	2.6	8.8	10	8.6	10.6	17.1	3.1	1.4	3.4	1.6	17.5
DS 5a	4.4	0.2	1.7	4.9	3.9	5.2	6.7	1.1	0.7	1.2	0.8	6.9
DS 6a	3.7	0.8	1.7	5.6	4.7	12.5	13.4	0.6	0.3	0.6	1.4	13.5
DS 7a	3	0.5	2.2	3.9	2	4.9	5.4	2	1.5	2.5	4.9	7.7
DS 8a	2.4	3.7	1.1	4.5	3.3	7.7	8.3	2.1	1.1	2.4	2.3	8.9
Coastal	9	7.3	4.5	14.9	12.1	22.6	27.7	4.9	2.7	5.5	15.4	32.2
DS 1b	1.8		0.3	1.8	0.3	0.1	0.3				1.1	1.1
DS 2b	2.4		0.4	2.4	0.6	0.2	0.6				2.9	3.0
DS 3b	3		0.5	3	1	0.3	1.1				2.1	2.4
DS 4b	3.4		0.6	3.5	1.5	0.3	1.5				1.6	2.2
DS 5b	3.5		2.9	4.5	1.1	0.3	1.2				0.8	1.4
DS 6b	3.4		5.1	6.1	1.2	0.4	1.2				1.4	1.8
DS 7b	2.8		0.7	2.9	1.8	0.6	2				4.9	5.3
DS 8b	2.4		0.7	2.5	0.9	0.4	1.1				2.3	2.5
interior	7.8		6	9.8	8.1	1.7	8.3				15.4	17.5
GrIS	11.9	7.3	7.5	17.8	14.5	22.7	28.9	4.9	2.7	5.5	0	29.4

TCD
9, 4661–4699, 2015

Table A3. The GIA effects on mass balance in different GrIS regions based on 11 different GIA models. The unit is Gt yr^{-1}. For the GIA models using Simpson's ice history model, the column headers are in the form of "xpab", where the *x* value refers to the lithosphere thickness, unit is km, and on the value of a and b represent the viscosity of the upper and lower mantle, the unit is 1020 (or 1021) Pa s, respectively.

ICE model	ICE-5G	Wouter van der Wal		Simpson							
Mascon	Paulson-07	heatflow	seismic	96p32	96p55	96p58	96p85	96p510	120p51	120p81	120p11
DS 1a	4	5	2	1	−1	−1	−1	0	3	4	4
DS 2a	3	1	1	1	1	1	2	2	2	3	3
DS 3a	0	2	−1	1	−1	−2	−1	−1	2	3	3
DS 4a	0	3	1	−1	0	0	1	1	1	3	4
DS 5a	−3	−1	0	−5	−8	−7	−7	−7	−4	−4	−5
DS 6a	−2	1	2	−5	−2	−2	1	−2	−3	−1	0
DS 7a	−3	0	0	−1	−5	−5	−6	−5	−2	−2	−3
DS 8a	−1	−1	0	1	−1	−2	−2	−2	−1	−2	−2
Ellesmere	7	4	4	1	2	3	4	3	4	5	6
Baffin	12	−3	6	10	12	12	12	13	1	0	−1
Iceland	−1	0	−1	−1	−3	−3	−3	−3	0	0	−1
Svalbard	2	0	2	2	3	4	3	5	0	0	0

TCD
9, 4661–4699, 2015